8-1-1984

Information theoretic metrics for the assessment of digital image-tone restored images

Paul W. Melnychuck

INFORMATION THEORETIC METRICS FOR THE ASSESSMENT OF DIGITAL IMAGE-TONE RESTORED IMAGES

by

Paul W. Melnychuck

B.S. Rochester Institute of Technology

(1982)

A thesis submitted in partial fulfillment
of the requirements for the degree of
Master of Science in the School of
Photographic Arts and Sciences in the
College of Graphic Arts and Photography
of the Rochester Institute of Technology

August, 1984

Signature of the Author Paul W. Melnychuck
Imaging and Photographic Science Dept.

Accepted by Ronald Francis
Coordinator, M.S. Degree Program

College of Graphic Arts and Photography
Rochester Institute of Technology
Rochester, New York

CERTIFICATE OF APPROVAL

M.S. DEGREE THESIS

The M.S. Degree Thesis of Paul W. Melnychuck
has been examined and approved
by the thesis committee as satisfactory
for the thesis requirement for the
Master of Science degree

Joseph H. Altman
Mr. Joseph H. Altman, Thesis Advisor

Peter Engledrum
Mr. Peter Engledrum

Rodney Shaw
Dr. Rodney Shaw

8/17/84
Date

James R. Sullivan
Mr. James R. Sullivan

THESIS RELEASE PERMISSION FORM
ROCHESTER INSTITUTE OF TECHNOLOGY
COLLEGE OF GRAPHIC ARTS AND PHOTOGRAPHY

Title of Thesis Information Theoretic Metrics for the Assessment of Digital Image-Tone Restored Images

I, Paul W. Melnychuck, prefer to be contacted each time a request for reproduction is made. I can be reached at the following address:

Eastman Kodak Company
Research Laboratories, B-82A
Rochester, New York 14650

Date 9/17/84

INFORMATION THEORETIC METRICS FOR THE ASSESSMENT OF DIGITAL IMAGE-TONE RESTORED IMAGES

by

Paul W. Melnychuck

Submitted to the
Imaging and Photographic Science Department
in partial fulfillment of the requirements
for the Master of Science degree
at the Rochester Institute of Technology

ABSTRACT

Digital image-tone restoration is examined in terms of information theoretic-based measurements. The metrics illustrate the relative degree of restorability of a 6-stop underexposure range on Kodak Tri-X pan film. An image chain model is developed to account for the discrete nature of sampled images used in digital image processing. The model includes the major system components (from object to viewed image) from which the system signal-to-noise ratio is calculated. Quantization noise and clipping are treated as signal-dependent, additive noise sources, and are shown to play a major role in degrading restored images. Although the eye characteristics are not included in the calculations, there is some indication that the logarithm of the information content and the noise equivalent number of quanta correlate with the visual perception of image quality of a restored pictorial image; these metrics demonstrate their utility in characterizing the practical limits of an image-tone restoration system.

ACKNOWLEDGEMENTS

This work would not have been possible without the significant contributions made by a number of kind individuals, whom I gratefully acknowledge:

Mr. J.H. Altman, for his patience, time and helpful suggestions in serving as my thesis advisor.

Mr. P.D. Burns, for his helful comments concerning the Wiener spectrum measurements.

Dr. P. Bunch & crew, for making the WS measurements.

Mr. G. Coutu, for his assistance and software.

Mr. P. Engledrum, for making me think.

Dr. J. DeLorenzo, for interesting discussions.

Dr. R. Francis, for all of his help over the years.

Mr. R.D. Lucitte, for many hours of assistance.

Mr. R. Mergler, for scanning the images.

Mr. S. Muratore, for all of his cooperation in scanning the images.

Dr. L. Ray, for his programming assistance.

Dr. R. Schaetzing, for the use of his software and for performing the 2-D FFT.

Dr. R. Shaw, for planting the seed.

Mr. J.R. Sullivan, for watering it.

and the management of the Image Recording Division of the Kodak Research Laboratories for their support of this work.

DEDICATION

This thesis is dedicated to my parents, Walter and Genoveva, my sister, Rosemary, and to those who have made a profound influence in my life.

CONTENTS

LIST OF ILLUSTRATIONS

INTRODUCTION

Tone-reproduction concerns mainly the macro-scale characteristics, the appearance of comparatively large areas, of an image. Many methods in tone-reproduction analysis have been developed, and the literature is extensive(1,2). The main objective of these methods is to devise criteria to distinguish between what may be termed "preferred" and "failed" tone-reproduction. Two important factors that influence the quality of tone-reproduction are the gradient, or contrast, and the dynamic range, or density range, of the system. Although these properties can be changed by a number of ways, this study addresses failed tone-reproduction as a result of underexposure, or moving the exposure range of the subject along the film's characteristic curve, towards the region where low levels of light exposure fail to form a developable latent image in the photographic material. In this region, a considerable change in exposure produces only slight changes in density, resulting in severe tone distortion of the underexposed image; there are fewer distinguishing tones recorded on the film than were present in the original subject. This tone-compression produces a rendition on the film that is too low in contrast ("flat") and the shadow areas lack detail.

Chemical methods to correct for failed tone-reproduction may involve a posterior intensification treatment of the developed image, to amplify the image densities to those which may result in a more preferred tone-reproduced image. Other chemical methods involve modified developer formulas called "push-processing" developers, or simply increasing the film development time. These techniques have been well documented by Haist(3). Chemical methods will yield a slight increase in film emulsion speed of negative films but with the risk of unwanted enhanced contrast, increased grain size, and other detrimental image characteristics.

Digital image processing offers flexibility that chemical analog techniques cannot afford. Whereas analog methods are constrained by physical phenomena, digital methods use mathematical manipulations via computers, and possess no constraints other than speed and cost.

Tone-scaling is a common digital image processing technique used to correct failed tone-reproduction, and can be found in standard texts such as Pratt(4) and Gonzalez and Wintz(5). Digital image-tone restoration is a tone-scaling technique which assumes a priori knowledge of the degree of exposure error (under or overexposure) for an image, and is used to correct failed tone-reproduction to preferred tone-reproduction, which presumably would resemble that of a normally exposed image. Tone

restoration differs from other forms of tone-scaling which are based on perceptual enhancement of the image, or to produce a desired density value distribution, or histogram. Although many applications of these techniques exist in the literature, the practical limit on the degree of underexposure that is restorable has not been reported. The purpose of this work is to describe the performance of a digital image-tone restoration system with respect to the relative degree of restorability, in terms of information theoretic metrics. These measurements will be compared with the visual assessment of a series of tone-restored pictorial images. It is not the intent of this work to maximize the tone restored results, but rather, to accept the quality of the generated images and simply construct a model to describe the image quality of the process which generated the output images.

Attempts to describe the image quality of a spatially recorded image date back to the early part of the century. A detailed account of the important advances in image analysis and evaluation can be found in Shaw(6) or Dainty and Shaw(7). More recent papers concerning image quality can be found in refs. 8 to 12. Numerous papers have shown the applicability of quantum-limited signal-to-noise metrics, such as detective quantum efficiency (DQE) and the noise equivalent number of available quanta (NEQ)

for the evaluation of photographic film, and imaging systems in general(13). The concept of NEQ provides a useful measure of image signal-to-noise and can be used as a metric for the assessment of image quality. Rose(14) demonstrated this by showing a series of images and the corresponding number of apparent photons used to record the image. In addition to describing the efficiency of radiation detectors, Schade(15) was prominent in establishing the Fourier approach to optical and photographic image evaluation. Higgins(16) reviewed the factors relating to image quality and showed the importance of using a log signal-to-noise metric, which is a form of information content.* Based on the work of Shannon(17), early application of information theory by Felgett and Linfoot(18), Jones(19), and Shaw(20), involved measuring the information capacity of emulsions, with a constant signal power spectrum being assumed. Kriss et al. (21) used a visually weighted information capacity metric to assess the quality of photographic images. Vendrovsky(22) showed that the logarithm of the information content is linearly related to subjective image quality. More

---

*I am grateful to Mr. J. R. Sullivan for bringing to my attention unpublished work on the use of information content since 1969.

recently, Fales, Huck, and Samms(23) used information content to assess the performance of image scanners. They used an assumed signal power spectrum shape and accounted for degradations such as aliasing and quantization which are present in digitally generated images.

The following section describes metrics for the evaluation of image-tone restoration performance. The theory begins with sensitometric-based metrics, progresses to signal-to-noise type metrics which include random fluctuations and deterministic noise sources, and leads to a derivation of information content.

THEORY

Digital Image-Tone Restoration

The objective of image-tone restoration is to correct a "failed" tone-reproduced image, to a "preferred" tone-reproduced image, via a monotonic remapping of the image densities. With a priori knowledge of the degree of exposure error (which is assumed or approximated), a density remapping function can be derived by selecting, for each density value in the degraded image, a new density value resembling a normally exposed image, according to the D-Log E curve of the recording film. The gain of the remapping function is then calculated as the ratio of the desired point gamma to that of the underexposed point gamma, where the point gamma is the first derivative of the D-Log E curve at a particular point. A series of functions can be derived for various degrees of exposure error, and this is shown in Figure 1 for Kodak Tri-X pan film. Note that the slope of the remapping function represents the point gain, or amplification, applied to the image. For low densities (shadows in the scene) the gain is high, and gradually approaches a value of unity towards higher negative densities. Intuitively this is reasonable, since we know there is very little

point gamma available as we extend out to the extreme toe region.

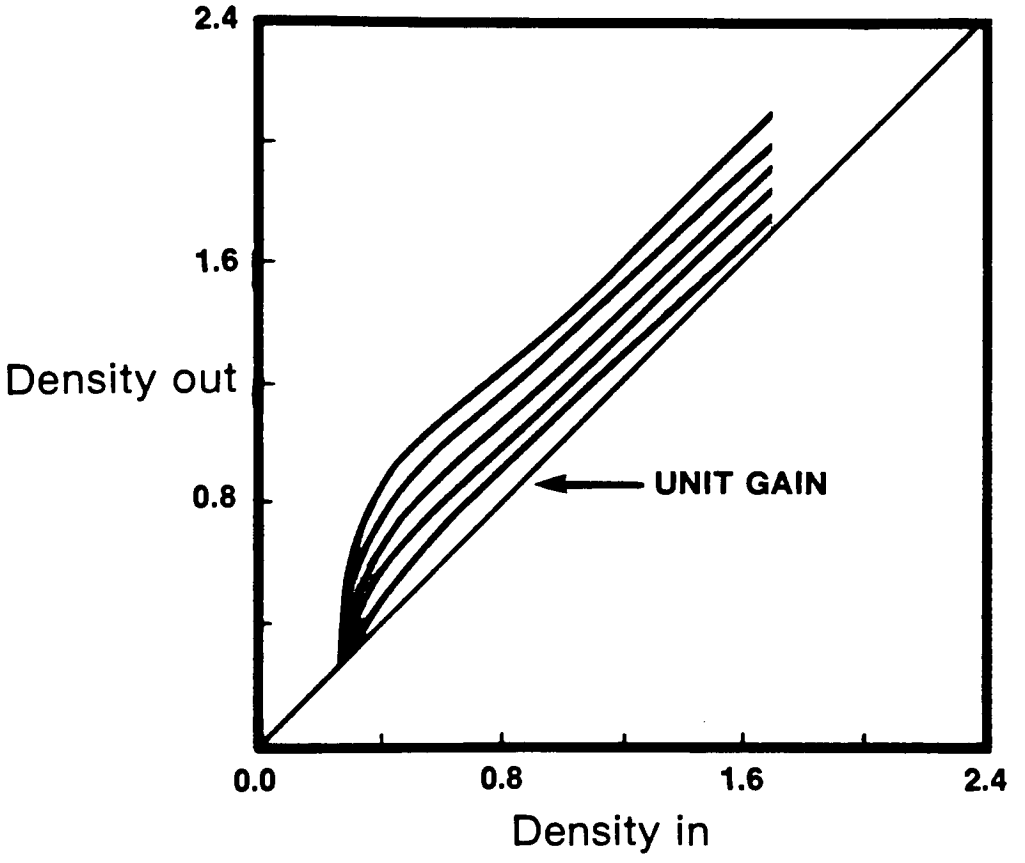

Figure 1. Density remapping functions for Kodak Tri-X pan film.

Film Point Gamma

Since image-tone restoration merely involves a density remapping, a simple first-order metric might be the point gamma of the remapping function. An evaluation of the point gamma as a function of exposure before and after tone restoration could be used to evaluate the overall success of the restoration; a perfect restoration would bring back a point gamma which would be identical to that for the normally exposed case. Figure 2 illustrates the point gamma as a function of exposure for progressive degrees of underexposure. The curves are placed so that the probability density distribution of the scene (in exposure space) is held fixed, while the curves are aligned to fall within the scene distribution. Additionally, the lowest exposure in the scene occurs 1 stop beyond the speed point of the film, which is how ANSI exposure meters are calibrated(24). For a nominal 6-stop (1.8 log exposure) input dynamic range, the available point gamma drops faster at low exposures, illustrating the effect underexposure has on shadow detail in the photograph.

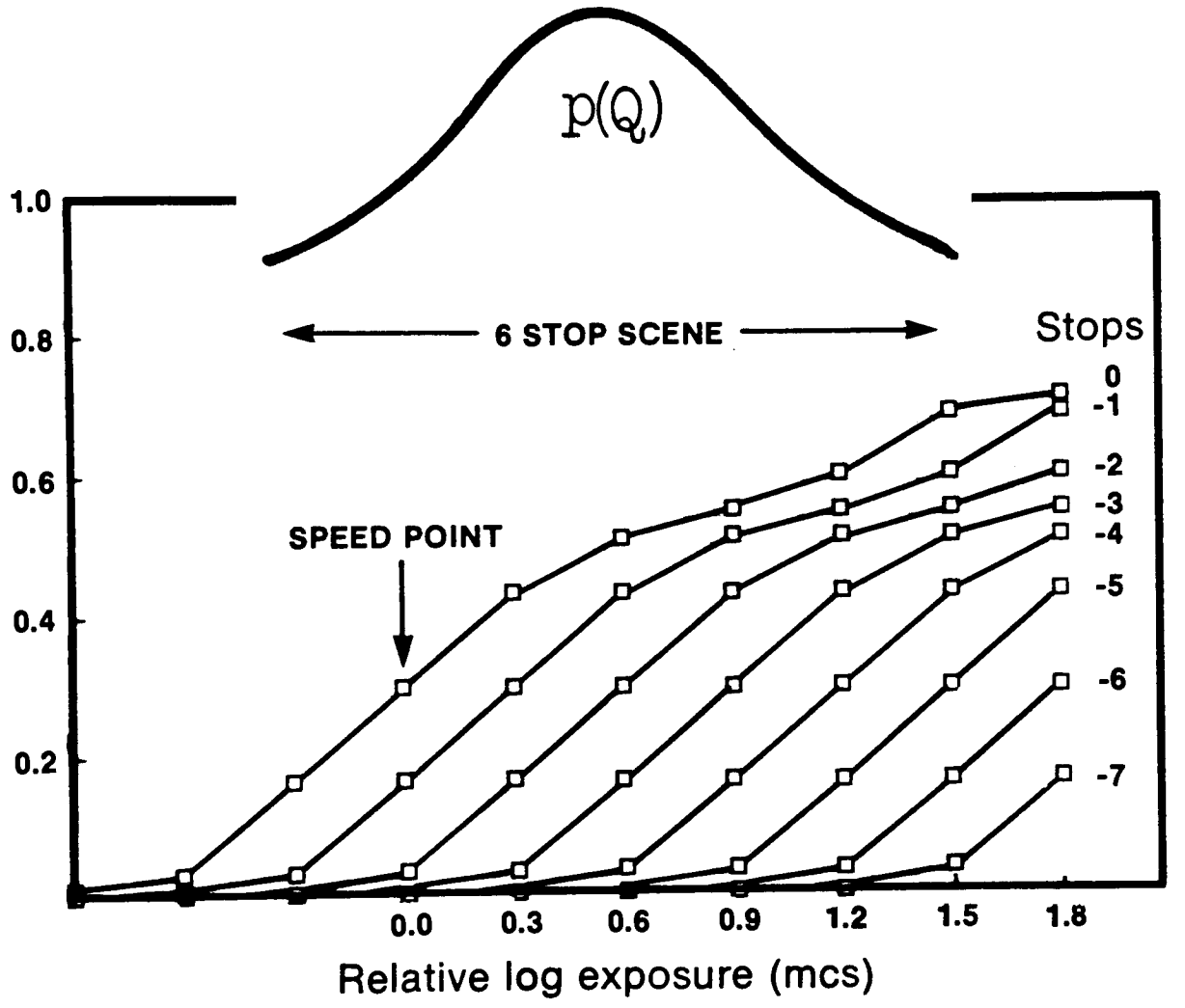

Figure 2. Point gamma available to record a 6-stop scene.

Effective Speed Gain

One method used to measure the sensitivity, or speed, in an imaging system is to measure its response at a specified density level. The American Standard method for measuring the speed of black-and-white films is to determine the exposure, E_m, corresponding to a density of 0.10 above base plus fog, when the film has been processed according to specified conditions. The speed is then computed by the relation

$$S = 0.8/E_m \qquad (1)$$

where E_m is stated in lux-seconds (meter-candle-seconds). A more complete definition of speed and sensitivity is given by Altman(25). Since the image-tone restoration process increases the densities in the low exposure, or shadow region (which is the area on the D-Log E curve where the speed point, or reference density, is most often specified) the result is an effective speed increase. Thus, the success of the image-tone restoration process can be tracked by measuring the effective exposure index, E.I., of the original recording film. Additionally, the E.I. can be used to compare its speed relative to that of other imaging systems where the speed is expressed in this

way. Although numerically there is an effective speed increase (in the sense that shadow detail is restored), in practice it is confounded for discrete images by the non-linear effects of quantization noise due to the digitization of the density levels. Because of this, the image may not in general exhibit a complete restoration of shadow detail. It is important to mention that this metric gives no indication of the image quality, or the consequences of extreme tone restoration with respect to preferred visual quality thresholds. In addition, this metric is a "DC" threshold descriptor that does not describe the micro-characteristics that are important to image quality.

Noise Equivalent Quanta (NEQ)

The performance of a radiation detector (one of which is a digital image-tone restoration system) can be described in terms of the signal-to-noise ratio (SNR) associated with the conversion of Q input quanta to output density, D. The detective quantum efficiency (DQE) defines the relationship between detector input and output fluctuations, when expressed in equivalent terms by translating the input exposure through the system gain:

$$DQE = \frac{\sigma_Q^2}{\sigma_D^2} \left(\frac{dD}{dQ}\right)^2 \qquad (2)$$

where σ_Q^2 and σ_D^2 are the variances of Q and D, respectively

As shown by Shaw(6), the concept of DQE leads to the possibility of expressing the output SNR of a detector as the noise-equivalent input, in terms of the noise-equivalent number of exposure quanta (NEQ). If the mean exposure, Q (in quanta/area), is assumed to follow Poisson statistics, $\sigma_Q^2 = Q$, and the SNR at the input of the detector may be defined as

$$SNR_{in}^2 = \left(\frac{Q}{\sqrt{Q}}\right)^2 = Q. \qquad (3)$$

For a practical detector the output SNR will be equivalent to the lesser number of quanta, NEQ, which defines the number of quanta an ideal detector would have needed to yield the same SNR.

$$SNR_{out}^2 = NEQ \qquad (4)$$

The DQE can now be expressed in terms of the NEQ

$$DQE = \frac{SNR^2_{out}}{SNR^2_{in}} = \frac{NEQ}{Q} . \qquad (5)$$

For photographic imaging systems the point gamma, $\hat{\gamma}(Q)$, can be approximated in terms of

$$\hat{\gamma}(Q) = \frac{dD}{d(\log_{10} Q)} = \frac{Q}{\log_{10} e} \left(\frac{dD}{dQ}\right) \qquad (6)$$

leading to

$$DQE = \frac{[\log_{10} e \ \hat{\gamma}(Q)]^2}{Q \ \sigma^2_D} . \qquad (7)$$

Following equation (5) the NEQ is then found to be

$$NEQ = \frac{[\log_{10} e \ \hat{\gamma}(Q)]^2}{\sigma^2_D} . \qquad (8)$$

If the density fluctuations are measured with an aperture of area A, the product $A\sigma^2_A$ is constant and

$$NEQ = \frac{[\log_{10} e^{\hat{\gamma}}(Q)]^2}{A\ \sigma_A^2} \tag{9}$$

where σ_A^2 is the measured variance.

Shaw has shown(6) that this is equivalent to

$$NEQ = \frac{[\log_{10} e^{\hat{\gamma}}(Q)]^2}{WS_N(0)}\ , \tag{10}$$

where $WS_N(0)$ denotes the very low frequency value, or scale value of the Wiener noise spectrum.

Since the variances at each spatial frequency are independent, equation (10) applies at all spatial frequencies so that the NEQ, as a function of spatial frequency, ω, is given(26) by

$$NEQ(Q,\omega) = \frac{[\log_{10} e^{\hat{\gamma}}(Q)MTF(\omega)]^2}{WS_N(Q,\omega)} \tag{11}$$

where $MTF(\omega)$ is the system modulation transfer function, which demodulates the output noise variance at each spatial frequency. The NEQ may also be expressed in terms of the contrast transfer function (CTF)

$$NEQ(Q,\omega) = \frac{0.189\ CTF^2(Q,\omega)}{WS_N(Q,\omega)} \tag{12}$$

where $CTF(Q,\omega) = \hat{\gamma}(Q)MTF(\omega)$. Equation (12) reveals that the NEQ is a generic descriptor of an imaging process that does not account for the signal itself, since the scene spectrum is not contained in the derivation. For this work, the NEQ was measured at the output stage of the tone restoration process and can be interpreted as the final noise equivalent number of available quanta in the tone restored images.

System Image Chain Model

In order to account for the discrete nature of sampled images used in digital image processing, an image chain model of the image-tone restoration system can be constructed by including quantization effects, aliasing, and the sequential noise and MTF components of the imaging process. In addition, it can be related to a "matched filter" metric for images by incorporating the input scene signal power spectrum. Figure 3 is a causal block diagram (27) representing the entire image-tone restoration process that includes the additive noise spectra and system transfer functions of each system component. The input, output, and sequential signal-to-noise ratios can be determined to analyze the image quality transfer throughout the system. With the assumption of additive

noise variances at each stage, and space invariant, linear transfer functions, the system S/N ratio is:

$$(S/N)^2 = \frac{S(\omega)\gamma_1^2\gamma_2^2\gamma_{i3}^2\gamma_4^2\gamma_5^2\gamma_6^2 MTF_1^2(\omega)MTF_2^2(\omega)MTF_4(\omega)^2 MTF_6(\omega)^2}{N_1(\omega)\gamma_2^2\gamma_{i3}^2\gamma_4^2\gamma_5^2\gamma_6^2 MTF_4^2(\omega)MTF_6^2(\omega)MTF^2(\omega) + N_2(\omega)\gamma_{i3}^2\gamma_4^2\gamma_5^2\gamma_6^2 MTF_4^2(\omega)MTF_6^2(\omega) + N_4(\omega)\gamma_5^2\gamma_6^2 MTF^2(\omega) + N_6(\omega)} \quad (13)$$

where:

$S(\omega)$	input Wiener signal spectrum
γ_1	original film gamma
γ_2	density to code value conversion
γ_{i3}	non-linear look-up table remapping
γ_4	code value to density conversion
γ_5	printing paper gamma
γ_6	eye gain
$MTF_1(\omega)$	original film MTF
$MTF_2(\omega)$	scanner MTF
$MTF_4(\omega)$	output writer/film MTF
$MTF_6(\omega)$	visual transfer function
$N_1(\omega)$	original film grain noise power spectrum
$N_2(\omega)$	quantization and clipping noise
$N_4(\omega)$	output film grain noise

$N_6(\omega)$ eye noise

Ignoring the eye characteristics, this reduces to

$$(S/N)^2 = \frac{S(\omega)\gamma_1^2\gamma_2^2\gamma_{i3}^2\gamma_4^2 MTF_1^2(\omega)MTF_2^2(\omega)MTF_4^2(\omega)}{N_1(\omega)\gamma_2^2\gamma_{i3}^2\gamma_4^2 MTF_2^2(\omega)MTF_4^2(\omega) + N_2(\omega)\gamma_{i3}^2\gamma_4^2 MTF_4^2(\omega) + N_4(\omega)} \quad (14)$$

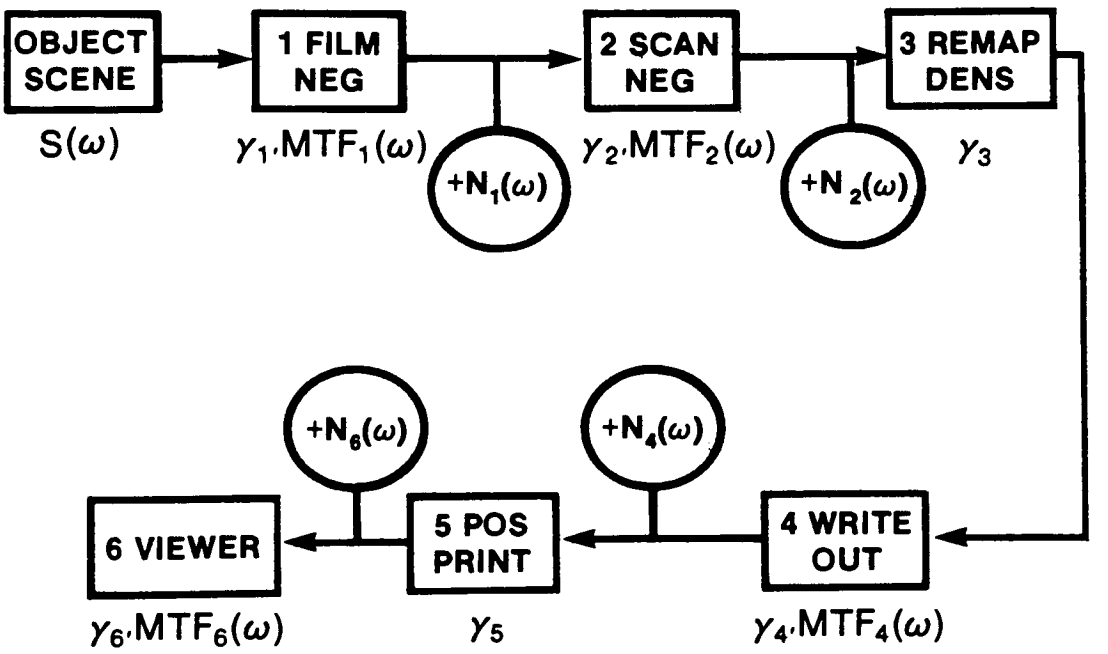

Figure 3. System image chain model for the image-tone restoration process.

The model assumes that there are no noise or MTF effects associated with the remapping (stage 3) and printing step

(stage 5) and that aliasing and banding artifacts are negligible. Because the human visual system has been ignored, the S/N ratio is not a function of the printing step (stage 5) and the analysis can be performed in terms of negative densities (stage 4). The first and last noise terms in the denominator of equation (14) can be directly measured from the output Wiener noise spectrum of uniform exposures because $N_1(\omega)$ and $N_4(\omega)$ are not spatially signal dependent. If $N_2(\omega)$ is set equal to zero, we are left with a signal-to-noise ratio that is due solely to the stochastic nature of the imaging process. The second noise term takes into account the discrete nature of the digitization process and allows for a more complete description of the stochastic and deterministic noise sources.

Quantization Noise and Clipping

Consider the shift in the probability density distribution of a scene (in exposure space) as a function of underexposure, as depicted in Figure 4. As the scene becomes increasingly underexposed, more of the scene is being recorded in the region of low point gamma. As the scene passes an exposure threshold, Q_t, where the resulting

density x_t, is the fog density, the scene information is lost, or truncated. Additionally, there is

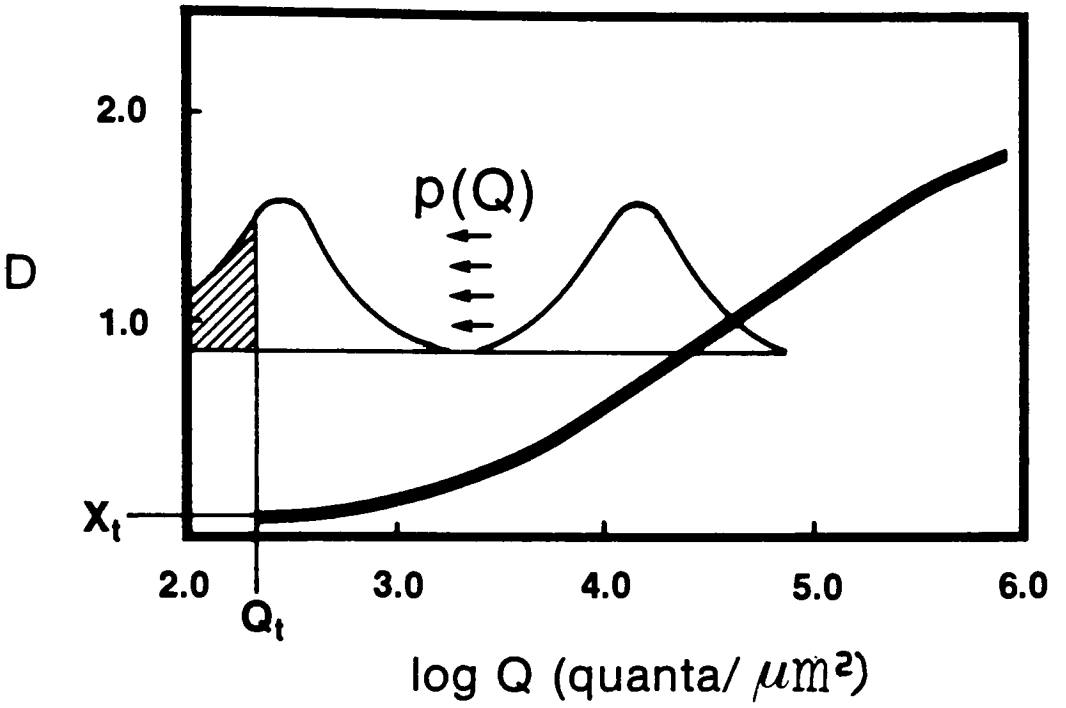

Figure 4. Shift in the probability distribution as a function of exposure

quantization error, which is defined as the mean squared difference between the true analog density, x_i, and the mean quantitized density, $\bar{x}_i$, summed over all quantization increments. The noise, denoted N_2, is considered here as a combination of quantization noise and amplitude

truncation, which will be referred to as clipping, and is treated as additive, signal-dependent noise. It is assumed that the image density amplitude is normalized to unity, and $p(x_i)$ is the probability density distribution of the input scene (translated into density space). For the purposes of deriving the quantization noise, Figure 5 illustrates an expanded view of the quantization increment, Δx_i, at a mean density level, $\bar{x}_i$.

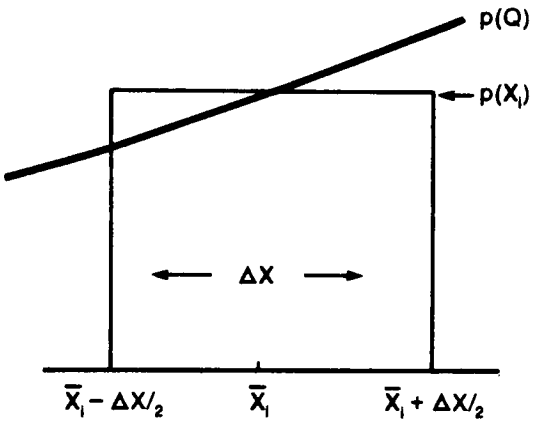

Figure 5. Expanded view of the quantization density increment.

The quantization error variance at the ith density level is (28):

$$\sigma_i^2 = \int_{\bar{x}_i - \Delta x_{i/2}}^{\bar{x}_i + \Delta x_{i/2}} (x_i - \bar{x}_i)^2 p(x_i) dx \,. \tag{15}$$

If we assume that $p(x_i)$ is constant within the quantization increment,* then

$$\sigma_i^2 = p(\bar{x}_i) \int_{\bar{x}_i - \Delta x_{i/2}}^{\bar{x}_i + \Delta x_{i/2}} (x_i - \bar{x}_i)^2 dx \,. \tag{16}$$

To facilitate the integration, let $u = (x_i - \bar{x}_i)$, leading to

$$\sigma_i^2 = p(\bar{x}_i) \int_{-\Delta x_{i/2}}^{-\Delta x_{i/2}} u^2 du \tag{17}$$

and, since the function is symmetric

---

*Note: This Riemman sum approximation is valid only for small quantization increments.

$$\sigma_i^2 = 2p(\bar{x}_i)\,\frac{u^3}{3}\Bigg|_0^{\Delta x_i/2} = \frac{(\Delta x_i)^3}{12}\,p(\bar{x}_i)\,. \tag{18}$$

Let the area under $p(\bar{x}_i)$, which is $\Delta x_i p(\bar{x}_i)$, be denoted P_i, which must sum to unity for all density levels, i.e., $\sum_i P_i = 1$; then

$$\sigma_i^2 = \frac{(\Delta x_i)^2}{12}\,P_i\,. \tag{19}$$

The total quantization error variance across all density levels is found by summing over all i:

$$\sigma_q^2 = \frac{1}{12}\sum_i (\Delta x_i)^2 P_i\,. \tag{20}$$

If the quantization levels are equally spaced across the density range, and if we apply a non-linear gain, γ_i, the total error becomes:

$$\sigma_q^2 = \frac{(\Delta x)^2}{12}\sum_i P_i \gamma_i^2\,. \tag{21}$$

Equation (21) reveals that the quantization error increases with the square of the gain. This shows that in

the limit of extreme tone restoration, the quantization error becomes a significant degradation term.* Since the clipped region is lost, and hence, not quantitized, the clipping error is simply the lost signal itself

$$\sigma_c^2 = \int_{\infty}^{x_t} x_i^2 \, P(x_i) dx \, . \tag{22}$$

and for the discrete case

$$\sigma_c^2 = \sum_i x_i^2 P_i \, . \tag{23}$$

We now wish to develop a functional form for $N_2(\omega)$ (also denoted $N_{q+c}(\omega)$), which represents the sum of the quantization noise power spectrum, $N_q(\omega)$, and the clipped signal power spectrum, $N_c(\omega)$. For the case of $N_c(\omega)$, the spectrum shape will be that given by the actual signal power spectrum, $S(\omega)$, with a variance given by equation (23). The shape of $N_q(\omega)$ is difficult to predict, and the

---

*Note: This will be visually noticeable in the tone restored image if the number of quantization levels are low. The visual effect can be minimized if the number of levels is increased, or a more efficient coding scheme, such as differential pulse code modulation (DPCM), is used(28).

only way of obtaining a reliable function is to measure it. For the purposes of this work, the shape of $N_q(\omega)$ was assumed to follow $S(\omega)$, which was measured and fitted to a function of the form

$$S(\omega) = \frac{b}{a + \omega^5} \tag{24}$$

Derivation of Information Content

In 1927 Hartley first proposed a quantitative measure whereby the capacities of different systems to transmit information may be compared. He defined the information capacity, C, of a system as the logarithm of the number of distinguishable states the system is capable of transmitting. If the logarithm is taken to the base 2, C is the capacity in terms of the number of binary storage units, or bits. In 1948 Shannon(29) laid the mathematical foundation for what has now become the field of information theory. Although the majority of the literature devoted to information theory has dealt with communication channels and the transmission of messages, the tools developed also apply to imaging systems; a concise treatment of the information theory approach to imaging systems is given by Shaw(6). In this section, an abbreviated derivation of information content is given from an imaging point of

view. For a more thorough discussion on the history, justification, mathematical properties and assumptions, and application of information theory, see refs. 30-33.

Shannon showed that the information received in a message Y about an event X is given as

$$\left[\begin{array}{c}\text{information} \\ \text{received}\end{array}\right] = \log \left[\begin{array}{c}\text{probability at the receiver of the} \\ \underline{\text{event after the message is received}} \\ \text{probability at the receiver of the} \\ \text{event before the message is received}\end{array}\right]$$

In the case of a perfectly reliable communication channel (i.e. no noise present) this reduces to

$$I = -\log\left[\begin{array}{l}\text{probability at the receiver of the event} \\ \text{before the message is received}\end{array}\right]$$

As an example, take a communication channel where a single letter of the alphabet is transmitted. If an "e" is transmitted and an "f" is received, the information, I, received is

$$I = \log \left[\begin{array}{l}\text{probability at the receiver that} \\ \text{an "e" was transmitted on the basis} \\ \underline{\text{of receiving an "f"}} \\ \text{a priori probability at the} \\ \text{receiver that an "e" was transmitted}\end{array}\right]$$

The use of the logarithm makes the quantity of information in independent messages additive, a property which is consistent with intuition. Further it is evident that

information is based on messages and is related to the degree of unexpectedness of the message. The less likely an event is to occur, the more information is contained in a message describing that event. Mathematically, information can be expressed in terms of the degrees of freedom in a system. Information is a function of the number of possible ways a message can occur. If a communication channel is capable of only transmitting the same message over and over again, there is no information being transmitted by that system. It can be shown that the total number of degrees of freedom in a communication system can be expressed as

DEGREES OF FREEDOM	=	# OF WAYS AN OUTPUT MESSAGE CAN OCCUR	X	PROBABILITY OF THE MESSAGE BEING RECEIVED
W	=	p(y)	X	p(y/x)

Similarly, we can describe the degrees of freedom in an imaging system as the product of the number of ways a system can generate a given image (histogram only) and the probability of occurrence of that image.

Consider an image as an ensemble of M pixels, or small resolution elements. Let p_i be the density level

probability density function (PDF) of the image and Mp_i, the number of observations, the ith density level, where i ranges from 1 to n density levels. Further, let f_i be the probability of observing the true signal value in a single pixel (it will be shown later that this is the nonzero-mean PDF of the noise). When $f_i = 1$ for all i, there is no uncertainty and each of the n density values occurs exactly as represented by the input image. Kikuchi and Soffer(34) showed that the total degrees of freedom, W, in the system is expressed as:

$$W = \frac{M!}{(Mp_1)!(Mp_2)!\ldots(Mp_n)!} f_1^{Mp_1} f_2^{Mp_2} \ldots f_n^{Mp_n} . \qquad (25)$$

This is the standard multinomial distribution, where $\Sigma_i p_i = 1$. According to Shannon, the information capacity of a transmitted message (or image) with W degrees of freedom is

$$I = \lim_{M\to\infty} \left(\frac{1}{M} \log_2 W\right) . \qquad (26)$$

Substituting for H we have

$$I = \lim_{M\to\infty}\left[\frac{\log_2 M!}{M} - \sum_{i=1}^{n} \frac{\log_2 (Mp_i)!}{M} + \sum_{i=1}^{n} \frac{Mp_i \log_2 f_i}{M}\right]. \qquad (27)$$

Applying Stirling's approximation (M is large)

$x! = \sqrt{2\pi x}\ (x/e)^x$, we have

$$I = \lim_{M\to\infty}\left[\frac{1}{M}\log_2\sqrt{2\pi M} + \frac{1}{M}M(\log_2 M - \log_2 e)\right.$$

$$- \sum_{i=1}^{n}\frac{1}{M}\log_2\sqrt{2\pi M p_i} - \frac{1}{M}M\sum_{i=1}^{n}p_i(\log_2 M p_i - \log_{10} e) \qquad (28)$$

$$\left. + \sum_{i=1}^{n} p_i \log_2 f_i\right] ,$$

which simplifies to

$$I = \lim_{M\to\infty}\left[\frac{1}{M}\log_2\sqrt{2\pi M} + \log_2 M - \log_2 e\right.$$

$$- \frac{1}{M}\sum_{i=1}^{n}\log_2\sqrt{2\pi M p_i} - \sum_{i=1}^{n} p_i \log_2 p_i - \log_2 M \sum_{i=1}^{n} p_i \qquad (29)$$

$$\left. + \log_2 e \sum_{i=1}^{n} p_i + \sum_{i=1}^{n} p_i \log_2 f_i\right]$$

If we apply the constraint $\sum_{i=1}^{n} p_i = 1$, and taking the limit as $M \to \infty$, yields

$$I = -\sum_{i=1}^{n} p_i \log_2 p_i + \sum_{i=1}^{n} p_i \log_2 f_i \qquad (30)$$

The first term in equation (30) is the entropy (or information) expression given by Shannon's second theorem, and is analogous to Boltzmann's entropy of a cell in statistical mechanics. Kikuchi and Soffer stressed that for a noisy channel, the entropy is given by both terms in equation (30), and it is this expression that is maximized in order to determine the most likely distribution for p_i.

Equation (30) allows the consideration of a communication channel (or imaging system) where an event (or object) X is received by a message (or image) Y, with the assumption of signal-independent, additive noise, n; this is illustrated in Figure 6a. It follows that the PDF of the signal, p_i, can be denoted p(y), and the PDF of the noise, f_i, be denoted p(y/x) (which is read, "the probability of the output y, given the input, x"). Equation (30) can now be rewritten as

$$I(x;y) = -\Sigma p(y)\log_2 p(y) + \Sigma p(y)\log_2 p(y/x) \qquad (31)$$

where I(x;y) is the information in x and y.

This, by definition, is

$$I(x;y) = I(y) - I(y/x) \qquad (32)$$

and represents the information about x contained in y. Equation (32) can be interpreted as the information of the event (or object) minus the information lost in the channel.

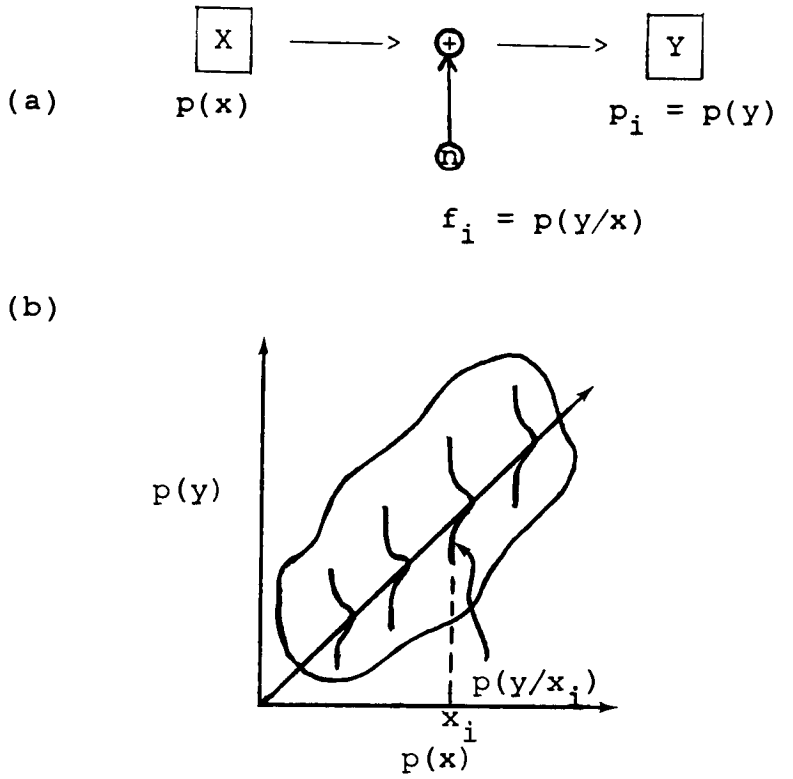

Figure 6. (a) Output of a system as an addition of signal plus noise, and (b) the mapping of p(x) to p(y).

Figure 6b illustrates the relationship between p(x) and p(y). If the PDF of receiving the output Y given the input X is a narrow distribution, the information lost in the system will be low and Y will be close to X. This is

so because p(y/x) represents the noise PDF, and any differences between p(y/x) and $\delta(y-x)$ (a one-to-one mapping) are due to the PDF of the noise being convolved with the PDF of the signal, to produce the PDF of Y, which reduces the amount of information transmitted through the system. The second term in equation (30) therefore reduces the degrees of freedom in the system, and thus does not allow as many possible images to be transmitted. We can think of a given scene as a sample of an ensemble of scenes whose probability is the reciprocal of the degrees of freedom, and the imaging system as an imperfect channel that will increase the probability of images, thereby lowering the information content.

We now proceed to determine the most likely PDF for p(y) and p(y/x), given constraints on the observed variances of the message(image) and the channel noise and, $\int_{-\infty}^{\infty} p(y)dy = 1$. Shannon used Lagrangian multipliers and stated the problem mathematically as

$$\max p(y) = \int_{-\infty}^{\infty} [p(y)\log p(y) + \lambda y^2 p(y) + \mu\, p(y)]dy \quad (33)$$

where λ and μ are normal Lagrangian multipliers. The condition for this maximum is

$$-1-\log p(y) + \lambda y^2 + \mu = 0 \ . \tag{34}$$

Solving for p(y) yields

$$p(y) = e^{-\mu} e^{-2y^2} \ . \tag{35}$$

The Lagrangian multipliers can be determined by applying the constraints

$$2e^{-\mu} \int_0^\infty y^2 e^{-\lambda y^2} \, dy = \sigma^2 \tag{36}$$

$$\int_{-\infty}^{\infty} p(y) dy = 1 \tag{37}$$

leading to

$$p(y) = \frac{1}{\sqrt{2\pi}\ \sigma} e^{-y^2/2\sigma^2} \tag{38}$$

which shows that the most likely distribution is a Gaussian. Similarly, p(y/x) is also found to be a Gaussian. Substitution of p(y) and p(y/x) into (31) yields

$$I(x,y) = \log_2(\sqrt{2\pi}\,\sigma_y) + \frac{\log_2 e}{2} - \log_2(\sqrt{2\pi}\,\sigma_n) - \frac{\log_2 e}{2} \quad (39)$$

which reduces to

$$I(x,y) = \frac{1}{2}\log_2\left(\frac{\sigma_y^2}{\sigma_n^2}\right). \quad (40)$$

Since the output signal Y is considered an addition of X and N, the variances add, and,

$$I(x,y) = \frac{1}{2}\log_2\left(\frac{\sigma_x^2 + \sigma_n^2}{\sigma_n^2}\right) = \frac{1}{2}\log_2\left(1 + \frac{\sigma_x^2}{\sigma_n^2}\right). \quad (41)$$

This relationship will hold at each spatial frequency and since all spatial frequencies are independent

$$IC = \frac{1}{2}\int_{-\infty}^{\infty}\int_{-\infty}^{\infty}\log_2\left[1 + \frac{S(u,v)}{WS_N(u,v)}\right]dudv. \quad (42)$$

where IC is now the information content in a unit area.

Fellgett and Linfoot(35) first applied equation 42 to photographic images. Assuming isotropy, the integral can be expressed in terms of a radial spatial frequency variable, $\omega = \sqrt{u^2 + v^2}$, to yield

$$IC = \pi \int_0^{\omega_c} \log_2 1 + \frac{S(\omega)}{WS_N(\omega)} \omega d\omega \qquad (43)$$

where ω_c is the cutoff frequency.

This is the familiar form of information content which shows that the information content in an image is related to the system signal-to-noise ratio. Dainty and Shaw have shown(36) that equation (43) can be stated in terms of the NEQ at a given mean exposure value Q

$$IC = \pi \int_0^{\omega_c} \log_2[1 + NEQ(Q,\omega)P(\omega)]\omega d\omega \qquad (44)$$

where $P(\omega)$ is the original signal power spectrum in exposure space (quanta^2•area). For this work the SNR given by equation (14) was used for the integrand in the information content calculations. Although the theory is developed for band-limited and not peak-limited systems (imaging is both) the information content is still a reasonable metric if one treats the peak-limited, or clipped, signal as a source of noise; the derivation of this was discussed earlier.

EXPERIMENTAL

The experimental effort has mainly involved the generation of images via the tone restoration scheme and measurement of the signal power spectrum and Wiener noise spectrum, from which the NEQ and information content were calculated.

Generation of Images

The original negatives were generated on 4x5 Kodak Tri-X pan film. The negatives were scanned with an Optronics drum scanner using a 100 μm square aperture, 50 μm square sampling, logarithmic amplifier, and 10 bit quantization; the data were stored on magnetic tape. The tone restoration step was performed on the coded density image via a look-up table of code values derived from remapping functions of the kind shown in Figure 1. Following the restoration, the code values were converted to digital voltage values which modulated an exposing source via a D/A converter, generating the output density image. The playback was also done on the Optronics using the same sampling parameters as in the scan mode, with one major exception which was that the D/A converter contained 8 rather than 10 bits. The output images were written

onto Kodak technical pan film in order to minimize the output film grain. The resulting negatives were contact-printed using conventional photographic methods. The entire scheme is shown in Figure 7; a similar digital imaging system is discussed in ref. 37, for example.

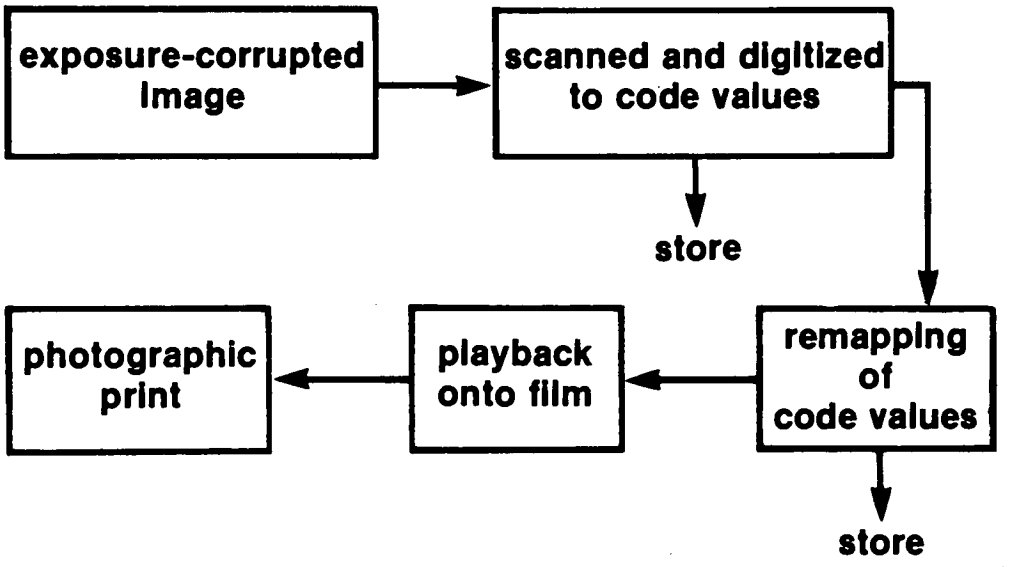

Figure 7. Digital image-tone restoration scheme.

Sensitometry

Uniform light exposures were made on a Kodak model Ib sensitometer using a simulated daylight source.

Fourteen samples representing the useful density range of the film were created for Wiener spectrum measurements and for input into the tone restoration process. The samples were treated identically to the actual images and were tone restored to the appropriate levels according to the desired remapping function for that level of underexposure. The end product was a series of uniform exposures made on the playback film for each underexposure case, to allow for the complete description of the noise as a function of density and degree of underexposure. The original Tri-X images were developed in undiluted Kodak developer D-76, as recommended by the manufacturer. The playback images were written onto Kodak technical pan film, type 2415, and were developed in Kodak HC-110 developer, dilution D, using tray development at room temperature.

MTF Measurements

As described in Figure 3 of the image-chain model, there are three MTF factors of concern in the system: the MTF of the original recording film, MTF_1, the MTF of the scanner, MTF_2, and the MTF of the playback writer, MTF_4 (assuming that the MTF of the Kodak technical-pan playback film is unity across the frequency range of interest

here). The MTF of the Kodak Tri-X pan film was measured at normal, 2, 4, and 6 stops underexposure using the sine-wave fringe method of Lamberts and Eisen(38). During scanning, the scanning aperture is generally smeared with a response envelope (rise, sustain, and decay) across each pixel; in this work this was approximated by a Dirac delta function. Additionally, the aperture function is generally convolved with the sampling lattice, which is represented by a lattice of delta functions. This results in a MTF in both the X and Y direction of

$$MTF(\omega) = \text{sinc}(0.100\pi\omega) \qquad (45)$$

Wiener Noise Spectrum Measurements

A description of the methods available for measurement of the Wiener spectrum for image noise analysis can be found in Dainty and Shaw(39). The equipment and procedure used for Wiener spectrum measurements in this study are those described by Bunch et al.(40). Here, only a brief description of the important measurement parameters follows.

A two-dimensional image density fluctuation, $\Delta D(x,y)$ existing over an image area (+X, +Y) has a Wiener spectrum defined by

$$WS(u,v) = \lim_{X,Y\to\infty} \left\langle \frac{1}{2X}\frac{1}{2Y} \left| \int_{-X}^{+X}\int_{-Y}^{+Y} \Delta D(x,y)\exp[-2\pi i(ux+vy)]dxdy \right|^2 \right\rangle$$

Assuming isotropy, and for direct digital calculation, the Wiener spectrum estimate is defined as

$$WS'(\omega) = \lim_{x\to\infty} \left| \frac{L}{X}\int_{-X/2}^{+X/2} \Delta D'(x)e^{-2\pi i\omega x}\,dx \right|^2 \qquad (46)$$

where L is the length of the measuring slit, X is the scan length, $\Delta D'(x)$ is the measured density fluctuation at the point x, and $WS'(\omega)$ is the measured Wiener spectrum. The measured Wiener spectrum is then related to the similarly biased input spectrum, $WS(\omega)$, by

$$WS'(\omega) = WS(\omega)MTF^2(\omega) \qquad (47)$$

where $MTF(\omega)$ is the transfer function of the measuring system. The practical measuring parameters of concern are the following:

- the sampling interval, Δx
- the total number of data values
- the scanning-slit dimensions

The Wiener noise spectrum measurements were made on a Perkin-Elmer PDS model 1010A microdensitometer dedicated to this purpose. Since both contact prints and 8x10 2X enlargements were to be made (to span the visual bandwidth assumed to be 10 cycles/mm at 1X), a Nyquist frequency of 20 cycles/mm was chosen to be appropriate for viewing. To help avoid aliasing, this necessitated a scanning aperture width of 25 μm, or larger; the actual slit dimensions used were 20x760 μm, which was experimentally convenient. Figure 8 shows the scanning scheme used in this study. To synthesize a suitably long scanning slit (in this case 8 x 0.76 mm = 6.08 mm) the original 131,072 transmittance readings were averaged across 8 physical slits, reducing the total number of points to 16,384, and the grand mean of the resulting array was subtracted from each value of the array. The array was segmented into 64 slices 40.96 mm long and a Wiener spectrum was then computed for each slice. The Wiener spectrum was the average across the slices and divided by the aperture function to arrive at the final Wiener noise spectrum.

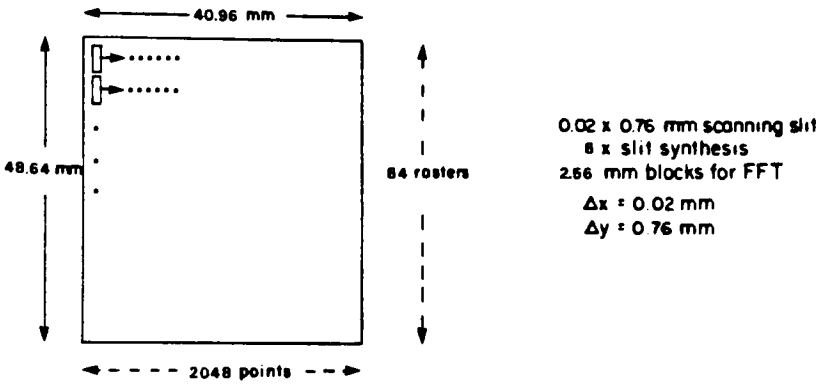

Figure 8. Wiener noise spectrum scanning scheme

The Wiener spectrum estimate is Chi-squared distributed, i.e., it is a random variable with an initial uncertainty that is reduced by replication. An estimate of the standard error, SE, for all but the zero and Nyquist frequencies is given by

$$SE = 1/\sqrt{N} \qquad (48)$$

where N is the number of blocks in the data stream. Because there is one less degree of freedom at the zero and Nyquist frequencies, the standard error at these frequencies is $\sqrt{2}$ higher than that at all others. For a 128 block stream, the SE's at zero and other frequencies are 12.5% and 9%, respectively.

Signal Power Spectrum & Probability Density Measurement

The object scene was assumed to be separable in the X and Y directions; a 512x512 two-dimensional FFT was performed on a region of the image (the woman's face) that was considered the most important in assessing the quality of the image. Since the separability assumption contradicts the isotropic assumption made earlier, and, since the signal-to-noise ratio was not considered from a directional standpoint, an average of the zero frequency X and Y direction signal power spectra was used in the analysis. This is a reasonable assumption for everyday scenes and the assumption has very little effect on the final results.

A code value histogram (linear with exposure) of the 8 bit output 512x512 array was made. Since code value is equivalent to exposure, the probability density function

in code value is equivalent to the probability density function in exposure.

Subjective Assessment of Images

Thirty observers were asked to assess the relative image-structure quality of the underexposed and tone restored images. The instruction given to the observers was to rate the degree of quality with respect to the amount of detail present in the woman's face, relative to that of the first (normally exposed) picture. The observers were instructed to give their ratings relative to a value of 100% for the normally exposed image.

RESULTS AND DISCUSSION

NEQ Measurements

Figure 9 shows the daylight sensitometric response of the Kodak Tri-X pan initial recording film; the exposure axis is given in log quanta/μm^2. If we assume that the scanning/playback system is capable of generating a unit slope (density in = density out) the characteristic curve at the output will be identical to that shown in Figure 9. The MTF of the Kodak Tri-X pan film was measured at a mean density of 1.0; Figure 10 shows the MTF response for increasing degrees of underexposure.

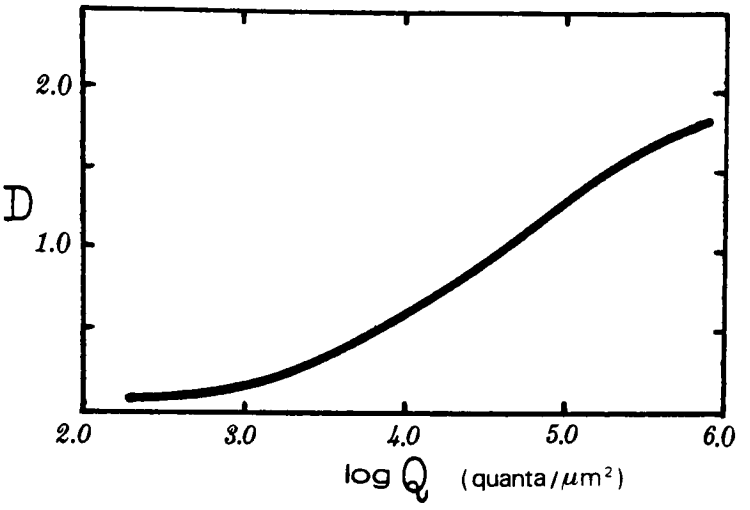

Figure 9. Sensitometric response of Kodak Tri-X pan film.

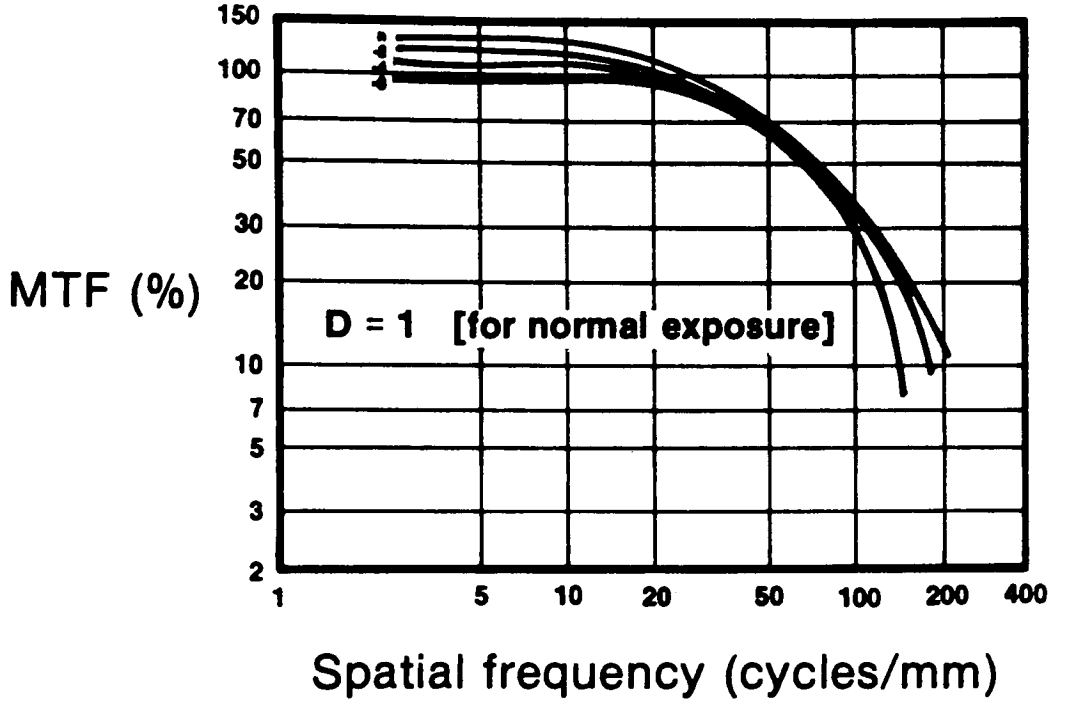

Figure 10. MTF of Kodak Tri-X pan film for various degrees of underexposure

---

Incorporating the scan and playback MTF's, the contrast transfer function can now be calculated at the output stage, and it is shown in Figure 11:

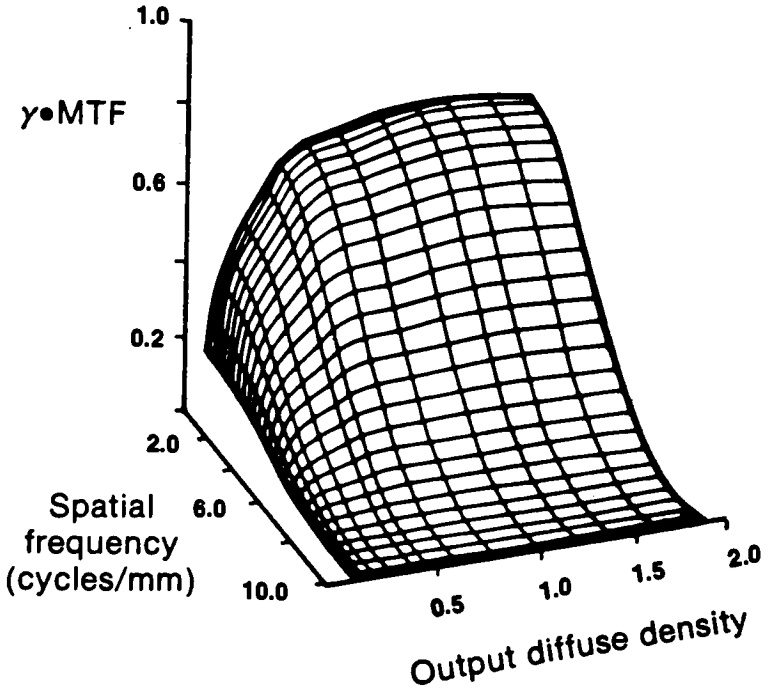

Figure 11. Contrast transfer function at output stage of system

The noise Wiener spectrum at the output stage is given in Figure 12.

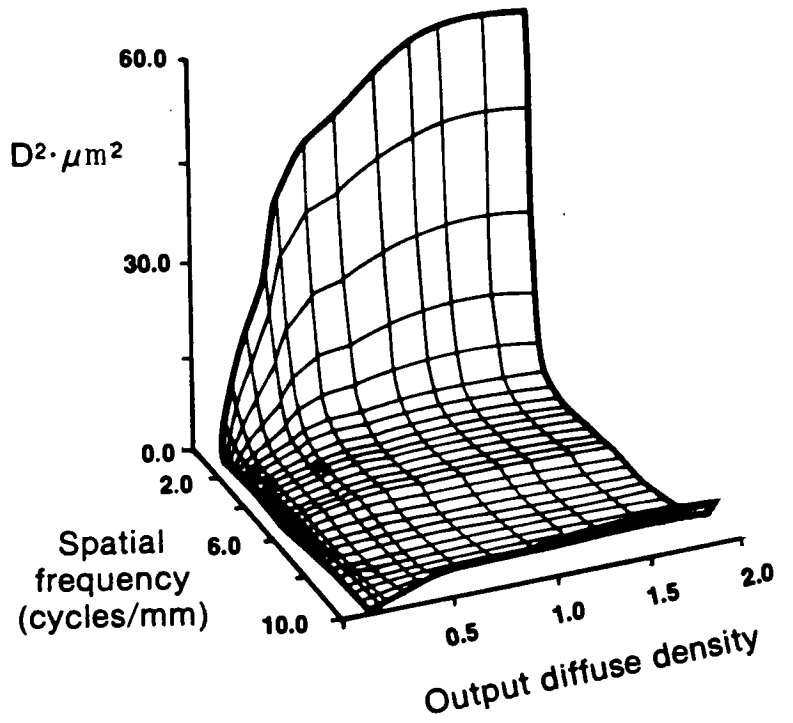

Figure 12. Measured Wiener noise spectrum at output stage of system

The CTF and Wiener spectrum surfaces may now be combined into the NEQ which allows for a concise description of the properties of an imaging system with respect to the spatial response and output density. The NEQ surface for each level of tone restoration is shown in Figure 17; alongside the surfaces are restored and unrestored

images. Note that the trend in the loss of NEQ with progressive degrees of tone restoration seems to follow the perceived degradation in image-structure quality of the tone restored images. Further, the order of magnitude of the NEQ (a maximum of about $0.04/\mu m^2$) is consistent with what would be expected from a moderate-quality conventional photographic system, whereas the highest quality would yield an NEQ approaching $1.0/\mu m^2$(41).

Calculation of Quantization Noise and Clipping

The scene probability density distribution (in code value) with its mean and variance in density is shown in Figure 13. It is this distribution that was used for the calculation of quantization noise and clipping variance, as described earlier. The total quantization and clipping variance at progressive degrees of tone restoration was calculated, and the results are shown in Figure 14.

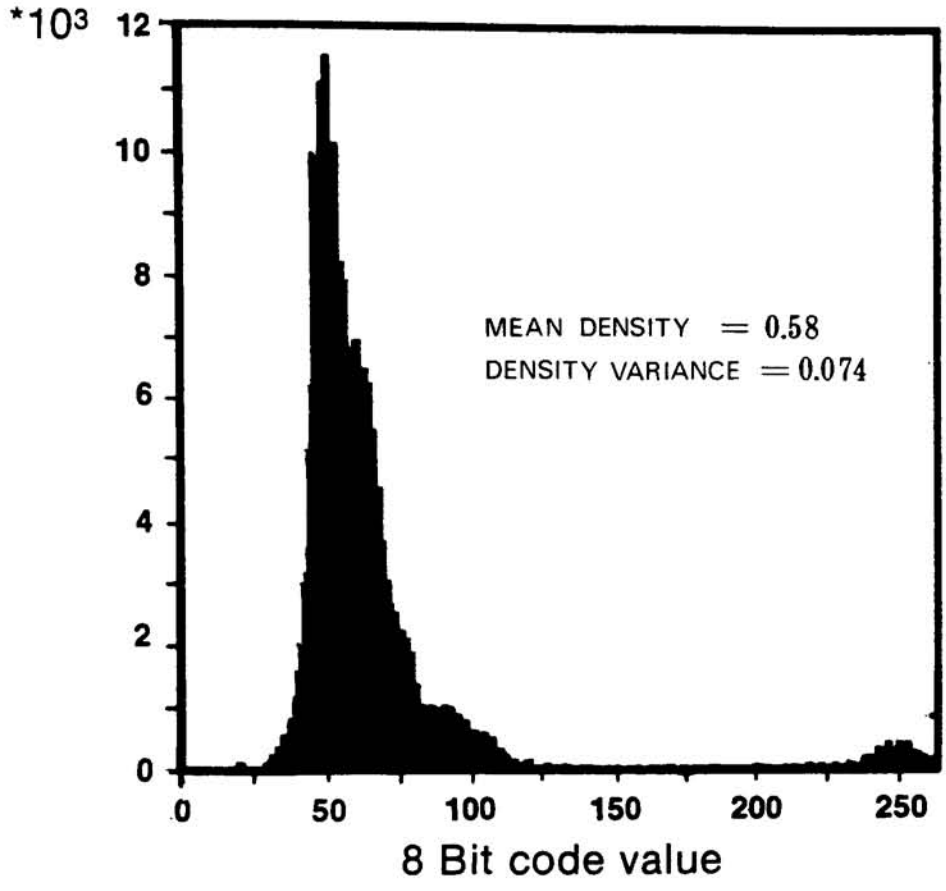

Figure 13. Scene probability density distribution.

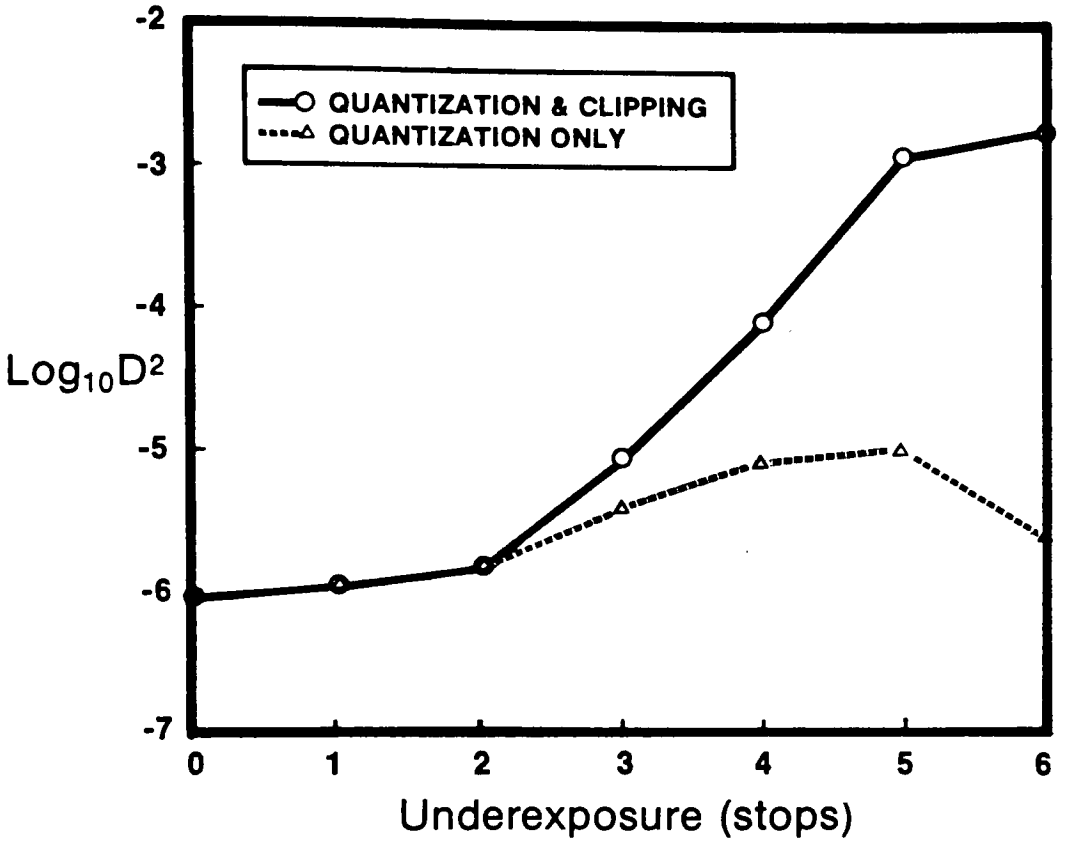

Figure 14. Total quantization noise and clipping variance.

The lower curve is the variance due solely to quantization noise. As the scene becomes more underexposed, less of the signal is quantized because a greater proportion is lost to clipping. The upper curve is the quantization and clipping variance, and shows that after three stops of underexposure, clipping becomes the major noise source.

As discussed earlier, $N_{q+c}(\omega)$ was assumed to follow the shape of the measured signal power spectrum, $S(\omega)$, with variances given by equations (21) and (23). The calculated spectrum, $N_{q+c}(\omega)$, can now be compared with the measured Wiener noise spectrum (which is signal independent, and thus contains no quantization or clipping noise) and with the measured signal power spectrum of the original scene, translated into density. For the normally exposed case, $N_{q+c}(\omega)$ has relatively low power compared with the Wiener noise and signal power spectrum. As we move towards a greater degree of tone restoration, the quantization and clipping noise become dominant and as Figure 15 illustrates, severely reduces the SNR; it is apparent that the majority of the signal exists below 3 cycles/mm. These calculated results are consistent with the observed degradation of quality in the images shown in Figure 17. It should be emphasized that the low power at high frequencies does not mean that the high-frequency information is unimportant. It simply means that because of low power, this information is especially vulnerable to the system noise and can be easily obscured by noise.

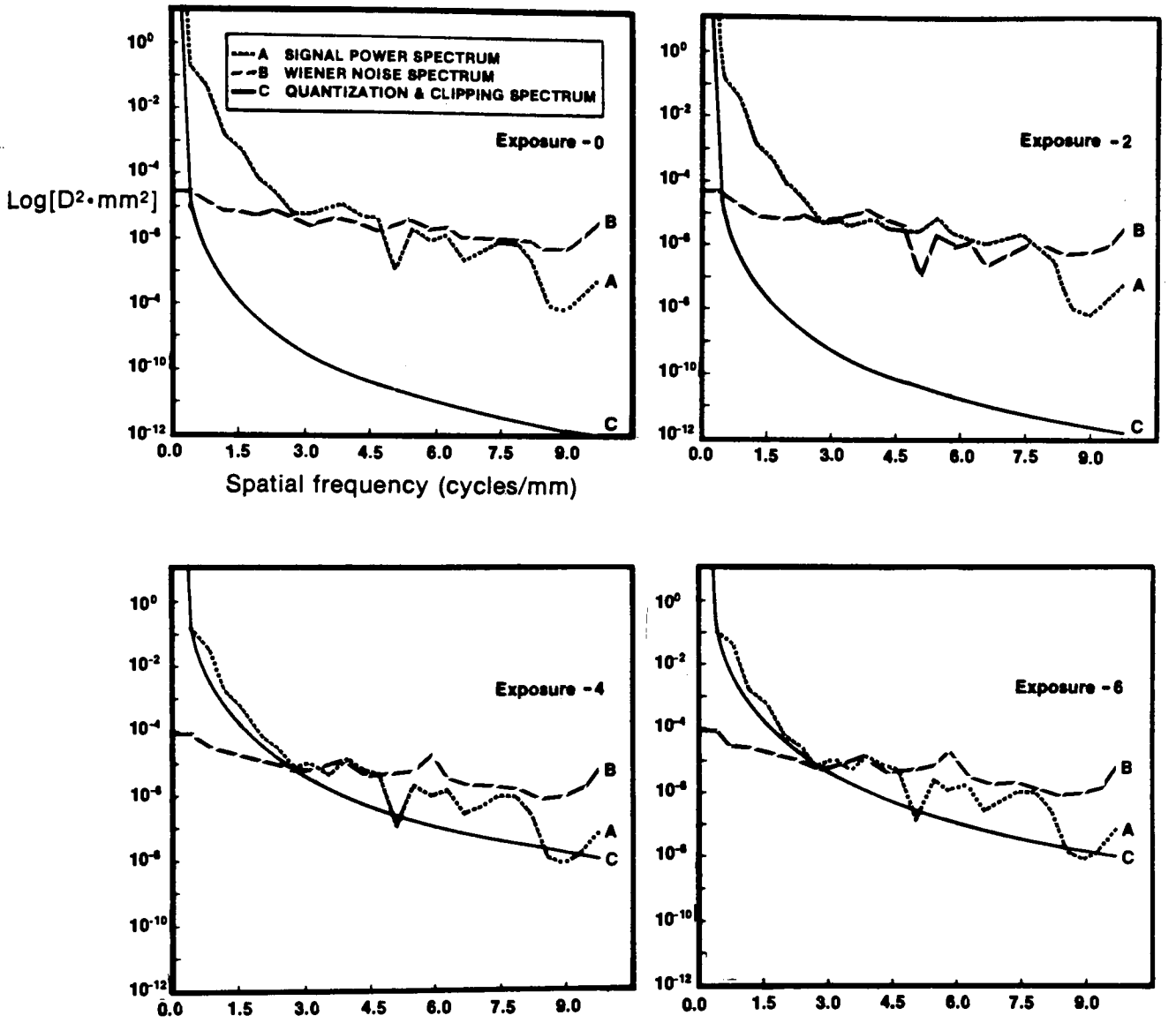

Figure 15. Comparison of Wiener spectrum with quantization + clipping noise.

Information Content Calculations and Images

Using the calculated signal-to-noise ratio given by the image chain model, the information content was calculated using equation (44). The NEQ trace representing the mean level of the scene was weighted with the original measured scene power spectrum to arrive at information content. The measured information content and log information content for each tone restored image are tabulated below:

stops underexposed	IC (bits/mm^2)	log IC (bits/mm^2)
normal	130	2.09
-1	123	2.09
-2	115	2.06
-3	90	1.95
-4	45	1.65
-5	27	1.43
-6	11	1.04

Figure 16. Information content for tone restored images.

These results are shown with the images in Figure 17 and compared with the visual assessment of underexposed and tone restored images in Figure 18.

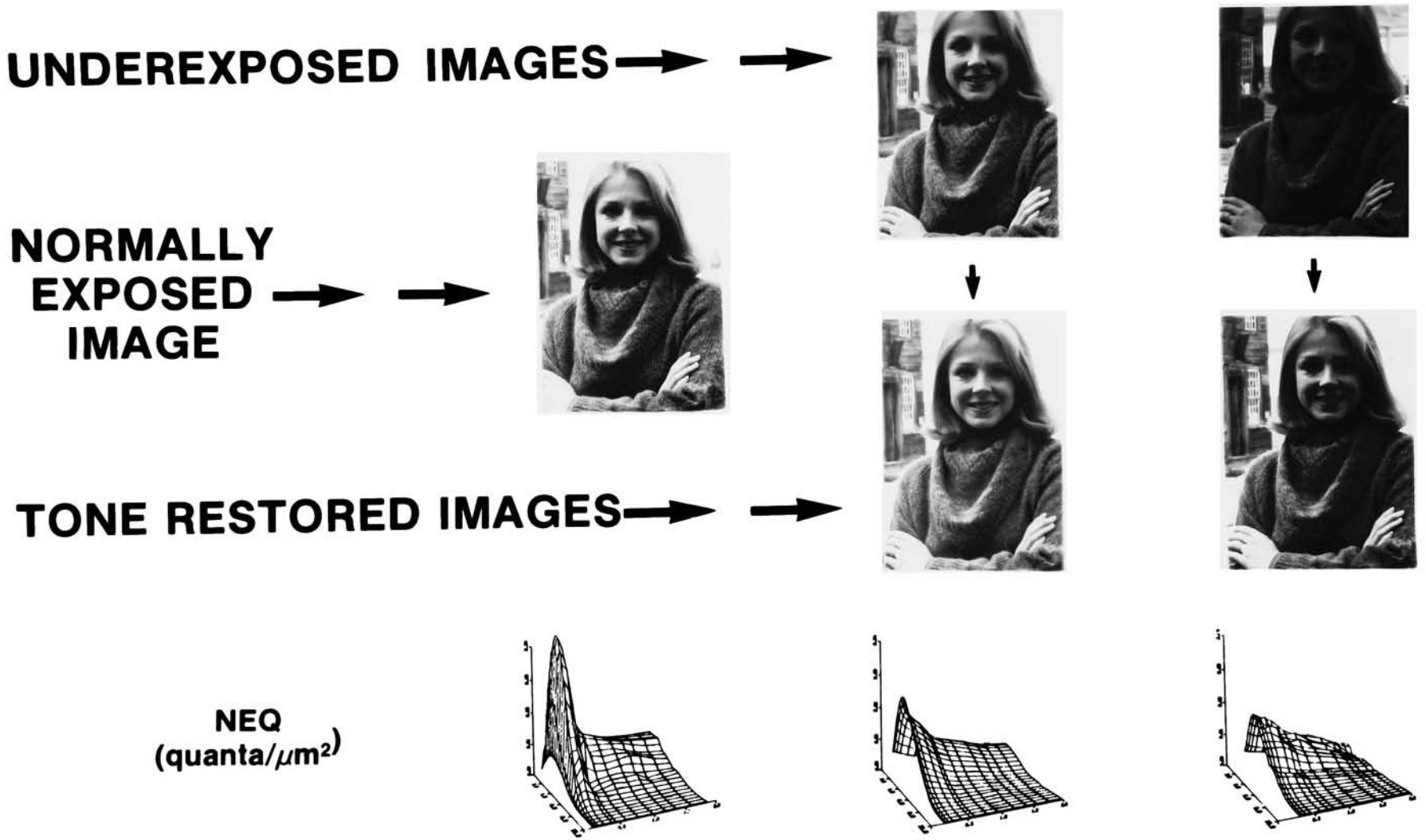
UNDEREXPOSED IMAGES
NORMALLY EXPOSED IMAGE
TONE RESTORED IMAGES
NEQ (quanta/μm^2)
INFORMATION CONTENT (IC) (bits/mm^2)
130
123
115
LOG_{10} [IC]
2.09
2.09
2.06
SUBJECTIVE RATING (%) (restored image)
100%
93%
86%

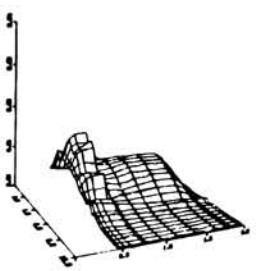

90

1.95

73%

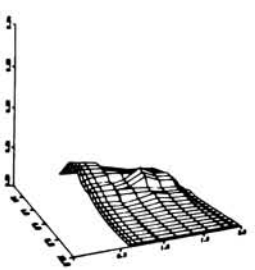

45

1.65

53%

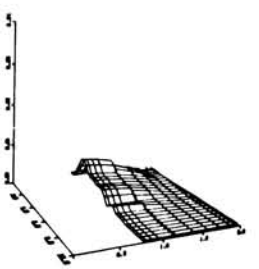

27

1.43

35%

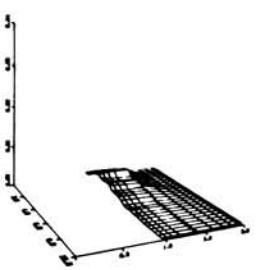

11

1.04

22%

Figure 18 does give some indication that the logarithm of information content correlates with the visual perception of image quality in the restored images. It should be stressed that although the eye perceived an information gain in the tone restored images (as is illustrated by the two lower curves), in fact, the actual information content in a tone restored image is less than or equal to that of the corresponding underexposed image. This is due to clipping, sampling, quantization, and playback degradations as well as the enhanced noise of the original underexposed image. The reason that the human observer perceives the restored image as having higher information despite the increased degradations is that the densities of the restored images are better matched to the dynamic range (and contrast sensitivity) of the eye. Since the sensitivity of the human visual system was not included in the model, it was necessary to eliminate this dynamic range factor by tonally restoring the images so that only the additional degradations included in the calculations would limit the perceived quality. If the sampling and playback system did not introduce degradations, an infinite number of bits were available, the original recording sensitometry never had a zero slope, and noise was not present, the restored images would have the same quality as the normally exposed image.

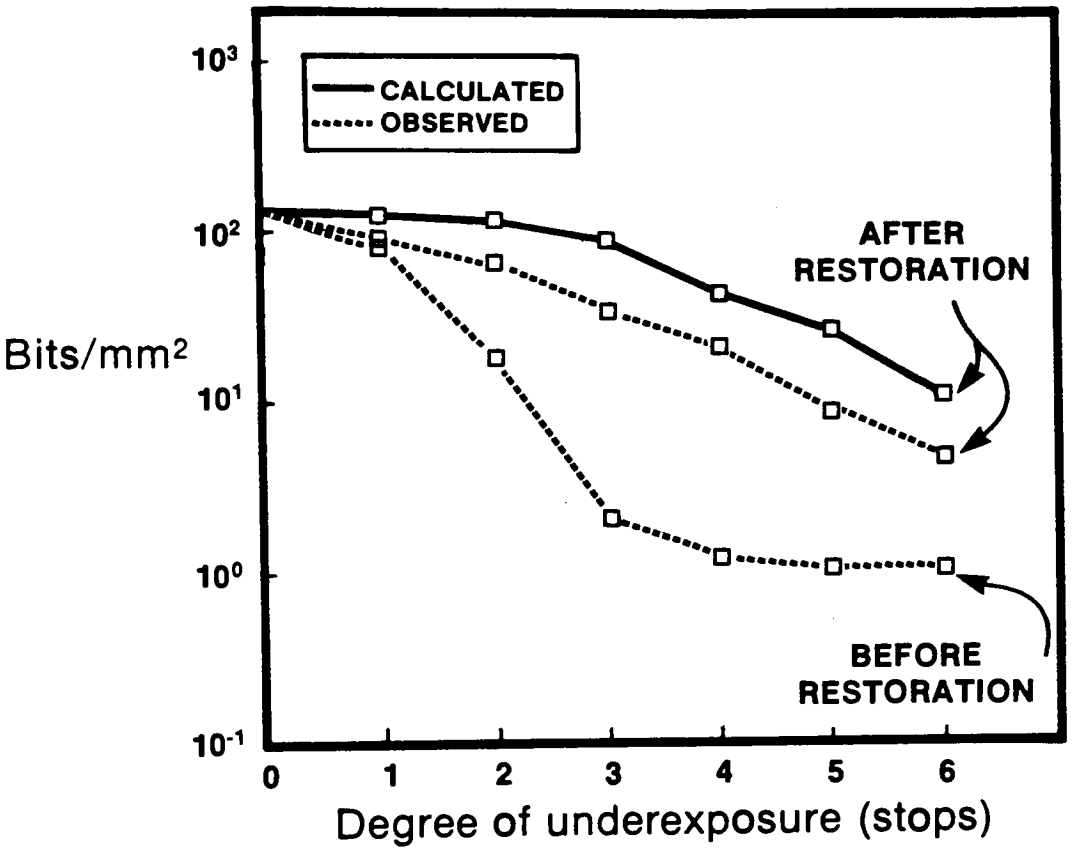

Figure 18. Log information content and subjective judgements vs degree of underexposure.

CONCLUSIONS

It has been shown that signal-to-noise metrics, information content and NEQ are useful in characterizing the performance of an image-tone restoration system. For discrete sampled images it was necessary to include degradations such as quantization noise and clipping, as they were found to be the major source of degradation in extreme tone restoration cases. The question of a real effective speed increase obtained by tone restoration was addressed. Although an effective speed increase is realized with tone restoration, it is difficult to quantify because it does not include the effect of quantization. In the light of the present and future use of photographic film as an initial recording medium for digital image processing, the speed alone of a film is not an adequate measure of a recording films's capabilities.

REFERENCES

1. C.N. Nelsen, in T. H. James, ed., The Theory of the Photographic Process, Macmillan, New York, 1977, ch. 19.

2. P. Kowaliski, Applied Photographic Theory, John Wiley and Sons, New York, 1972, ch. 1.

3. G. Haist, Modern Photographic Processing, Vol. 1 and 2, John Wiley and Sons, New York, 1979.

4. W.K. Pratt, Digital Image Processing, John Wiley & Sons, New York, 1978, pp. 307-311.

5. R.C. Gonzalez and P. Wintz, Digital Image Processing, Addison-Wesley, Reading, Mass., 1977, pp. 118-139.

6. R. Shaw,"Evaluating the Efficiency of Imaging Processes," Rep. Prog. Phys. 41: 1103-1155 (1978).

7. J.C. Dainty and R. Shaw, Image Science, Academic Press, New York, 1974.

8. R. Shaw, ed., Selected Readings in Image Evaluation, SPSE (1976).

9. R. Shaw, ed., Image Analysis and Evaluation, SPSE Conference, Toronto (1976).

10. P.S. Cheatham, ed., Image Quality, SPIE Proc., vol. 310, San Diego (1981).

11. International Congress of Photographic Science Proc., SPSE, Rochester (1978).

12. M. Kriss, in T.H. James, ed., The Theory of the Photographic Process, Macmillan, New York, 1977, ch. 21.

13. J.C. Dainty and R. Shaw, op. cit., ch. 5.

14. A. Rose, "The Dependence of Image Quality on Quantum Efficiency in Available Light Photography," in R. Shaw, ed., Image Analysis and Evaluation, SPSE Proc., Toronto (1976).

15. O.H. Schade, "An Evaluation of Photographic Image Quality and Resolving Power," J. Soc. Motion Pict. Tel. Eng., 73: 81 (1964).

16. G. Higgins, "Image Quality," J. Appl. Photogr. Eng. 3: 53-60 (1977).

17. C. Shannon, "A Mathematical Theory of Communication," Bell Syst. Tech. J. 27: 379 (1948).

18. P.B. Felgett and E.H. Linfoot, "On the Assessment of Optical Images," Phil. Trans. Roy. Soc. London, Ser. A 247: 369-407 (1955).

19. R.C. Jones, "The Information Capacity of Photographic Films," J. Opt. Soc. Am. 45: 799 (1955).

20. R. Shaw, "The Application of Fourier Techniques and Information Theory to the Assessment of Photographic Image Quality," Photogr. Sci. Eng. 6: 281-286 (1962).

21. M. Kriss, J. O'Toole, J. Kinard, "Information Capacity as a Measure of Image Structure Quality of the Photographic Image," (see ref. 6).

22. K.V. Vendrovsky, et al., "Information Content of B/W and Color Images," ICPS Proc., 1978.

23. C.L. Fales, F.O. Huck, R.W. Samms, "Imaging System Design for Improved Information Capacity," Appl. Opt., 23: 872-888 (1984).

24. J.H. Altman, in T.H. James, ed., The Theory of the Photographic Process, Macmillan, New York, 1977, pp. 507-509.

25. J.H. Altman, ibid., p. 508.

26. R. Shaw, "Photon Fluctuations, Equivalent Quantum Efficiency, and the Information Capacity of Photographic Images," J. Phot. Sci. 11: 313-320 (1963).

27. See, for example: G.R. Cooper and C.D. McGillem, Methods of Signal and System Analysis, Holt, Rinehart, New York, 1967, ch. 8.

28. W.K. Pratt, op. cit., p. 142.

29. C. Shannon, op. cit.

30. A.I. Khinchin, Mathematical Foundations of Information Theory, Dover, New York, 1957.

31. S. Goldman, Information Theory, Prentice-Hall, New York, 1953.

32. P.M. Woodward, Probability and Information Theory with Applications to Radar, Pergamon Press, Oxford 1953, ch. 3.

33. B.R. Frieden, Probability, Statistical Optics, and Data Testing, Springer-Verlag, New York, 1983, ch. 10.

34. R. Kikuchi and B.H. Soffer, "Maximum Entropy Image Restoration. The Entropy Expression," J. Opt. Soc. Am. 67: 1656-1665 (1977).

35. P. B. Fellgett and E. H. Linfoot, op. cit.

36. J.C. Dainty and R. Shaw, op. cit., ch. 10.

37. J.E. Boyd, "Digital Image Film Generation--From the Photoscientist's Perspective," J. Appl. Photo. Eng. 8: 15-22 (1982).

38. R.L. Lamberts and F.C. Eisen, "A System for Automated Evaluation of Modulation Transfer Functions of Photographic Materials," J. Appl. Photogr. Eng. 6: 1-8 (1980).

39. J.C. Dainty and R. Shaw, op. cit., ch. 8.

40. P.C. Bunch, R. Shaw, R.L. Van Metter, "Signal-to Noise Measurements for a Screen-Film System," SPIE Proc., San Diego (1984).

41. J.C. Dainty and R. Shaw, op. cit.

VITA

Paul W. Melnychuck was born in 1960 in Yonkers, New York, and lived in Mohegan Lake, New York, for most of his life. In 1978 he attended the Rochester Institute of Technology and in 1980 received the A.A.S. in Photographic Science, in 1982 the B.S. in Chemistry, and in 1984 the M.S. in Imaging and Photographic Science. While at RIT, Paul was employed with Eastman Kodak Company for three years as a cooperative education student. Presently, he is with the Image Analysis Group of the Kodak Research Laboratories.